



Analysis of tissue-substrate adhesion by hyperspectral surface plasmon resonance microscopy

Bo Yang^{1,2} · Hongyi Tang^{1,2} · Ziwei Liu⁴ · Xinxia Cai^{1,2} · Zhi-mei Qi^{1,2,3}

Received: 24 May 2024 / Revised: 8 August 2024 / Accepted: 12 August 2024
© The Author(s), under exclusive licence to Springer-Verlag GmbH, DE part of Springer Nature 2024

Abstract

The preparation of histology slides is a critical step in histopathology, and poor-quality histology slides with weak adhesion of tissue sections to the substrate often affect diagnostic accuracy and sometimes lead to diagnostic failure due to tissue section detachment. This issue has been of concern and some methods have been proposed to enhance tissue-substrate adhesion. Unfortunately, quantitative analysis of the adhesion between tissue sections and glass slides is still challenging. In this work, the adhesion of mouse brain tissue sections on gold-coated glass slides was analyzed using a laboratory-fabricated hyperspectral surface plasmon resonance microscopy (HSPRM) system that enabled single-pixel spectral SPR sensing and provided two-dimensional (2D) distribution of resonance wavelengths (RWs). The existence of the nanoscale water gap between the tissue section and the substrate was verified by fitting the RW measured in each pixel using the five-layer Fresnel reflection model. In addition, a 2D image of the tissue-substrate adhesion distance (AD) was obtained from the measured 2D distribution of RWs. The results showed that tissue-substrate AD was 20–35 nm in deionized water and 4–24 nm in saline solution. The HSPRM system used in this work has a wide wavelength range of 400–1000 nm and can perform highly sensitive and label-free detection over a large dynamic detection range with high spectral and spatial resolutions, showing significant potential applications in stain-free tissue imaging, quantitative analysis of tissue-substrate adhesion, accurate identification of tumor cells, and rapid histopathological diagnosis.

Keywords Hyperspectral surface plasmon resonance microscopy (HSPRM) · Resonance wavelength (RW) · Tissue section · Adhesion distance (AD) · 2D image of AD

Introduction

Histopathology is the gold standard for clinical diagnosis of tumors and cancers, and it requires staining and fixation of tissue sections to form histology slides for microscopy

image analysis. Staining is a complex and time-consuming process that may negatively affect the intrinsic properties of tissues. This issue has attracted attention, and a recent innovative work shows a plasmonically active microscope slide referred to as nanoslide for stain-free histopathology [1]. This type of nanoslide can provide a color image of an unstained tissue section to distinguish between diseased and normal areas of tissue. However, the preparation of such nanoslides is complex and time-consuming, resulting in high testing costs. In addition to staining, the adhesion of tissue sections to glass substrates is also a focus of concern in the preparing process of histology slides. Poor-quality histology slides with weak adhesion of tissue sections often affect diagnostic accuracy and sometimes lead to diagnostic failure due to tissue section detachment [2]. Various methods have been used to enhance the adhesion of tissue sections to slides, including (but not limited to) using adhesives, modifying the slide surface, and reducing the section thickness. At present, there is a lack of effective means to analyze

✉ Zhi-mei Qi
zhimei-qi@mail.ie.ac.cn

¹ State Key Laboratory of Transducer Technology, Aerospace Information Research Institute, Chinese Academy of Sciences, Beijing 100190, China

² School of Electronic, Electrical, and Communication Engineering, University of Chinese Academy of Sciences, Beijing 100049, China

³ College of Materials Science and Opto-Electronic Technology, University of Chinese Academy of Sciences, Beijing 100049, China

⁴ Beijing Smartchip Microelectronics Technology Co., Ltd, Beijing 102200, China

the adhesion strength of tissue sections to glass slides [3]. Therefore, it is necessary to develop new methods for quantitative analysis of tissue-substrate adhesion and stain-free histopathological diagnosis. In this work, the label-free and quantitative analysis of the adhesion of tissue sections to the gold-covered glass slides was implemented for the first time using the laboratory-fabricated hyperspectral surface plasmon resonance microscopy (HSPRM) system.

SPR imaging (SPRi) sensor is a typical label-free bioanalyzer with high sensitivity and high throughput, which enables biodetection based on the interaction of surface plasmon wave (SPW) propagating at the metal/dielectric interface with biological analytes bound on the interface [4]. Since the first SPRi sensor was reported in 1987 [5], this type of sensor has been extensively studied. Nowadays, SPRi sensors are commercially available, and they have been widely used in the fields of biochemical detection [6], drug research [7], food safety [8], and clinical diagnosis [9]. SPRi sensors have been proven to be sensitive enough to distinguish cancer cells from normal cells based on small differences in refractive index (RI) between them [10]. This means that the SPRi sensor is in principle capable of identifying cancerous areas in tissue sections when used for histopathological diagnosis. However, to the best of our knowledge, there are no reports of using the SPRi sensor for non-staining analysis of tissue sections, and the biosamples detected with SPRi sensors are concentrated on particulates including cells, viruses, bacteria, exosomes, and biomolecules [11]. Most existing SPRi devices operate at a fixed angle of incidence with a laser light source and provided grayscale images, and they are used to achieve RI detection of individual living cells [12]. Such devices have a narrow dynamic detection range, typically around 0.02 RIU [13], making it quite difficult to detect biological tissue sections as the RI difference between different sites within tissue sections is often greater than 0.02 [14]. Recently, a wavelength-modulated SPRi sensor has been developed that provides resonance wavelength (RW) images for the analysis of cell-substrate adhesion [15], and this sensor has the spectral sampling interval of 3 nm and the spectral range of 620–680 nm. According to the reference, the RI sensitivity of the spectral SPR sensor is approximately 3550 nm/RIU [16]. In the case of this sensitivity, the 60-nm bandwidth of the wavelength-modulated SPRi sensor corresponds to a dynamic detection range of 0.017 RIU. This range is too narrow to make the sensor suitable for stain-free analysis of tissue sections. In order to achieve stain-free analysis of tissue sections using a spectral SPRi sensor, the sensor should have a broad bandwidth for a wide dynamic detection range while keeping high sensitivity. Fortunately, we have recently developed a broadband spectral SPRi sensor with single-pixel resolved high sensitivity, which was prepared by combining a hyperspectral microscope

with a Kretschmann-type spectral SPR sensor [17]. This is a new class of powerful label-free sensors called HSPRM system, which is capable of monochrome and multicolor SPR imaging and single-pixel spectral SPR sensing, as well as two-dimensional (2D) quantitative characterization of thin films using measured RW images. The HSPRM has a wide spectral range of 400–1000 nm with a spectral resolution of up to 0.41 nm, and its spatial resolution along the SPW propagation direction is up to 2 μm . With these unique features, the HSPRM system is an ideal platform for quantitative analysis of unstained tissue sections.

In this work, the HSPRM was used for the first time to achieve a stain-free analysis of the adhesion of biological tissue sections on gold-covered glass slides. Mouse brain tissue sections were prepared as analytes, and they were attached to the SPR chip with deionized water. The RW images were measured with the mouse brain tissue-attached SPR chip and then fitted based on the five-layer Fresnel reflection model. A single-pixel resolved nanoscale gap between the tissue sections and the SPR chip was quantified, and the 2D distribution of the tissue-substrate adhesion distance (AD) was determined. Adhesion of the mouse brain tissue section to the SPR chip with saline solution instead of deionized water results in a decreased AD. The measurement process is described in detail below.

Materials and methods

Sample preparation

SPR chip The substrates used are ZF7LA (corresponding to SF6 Schott glass) glass slides with polished surfaces, and they were sequentially sonicated with acetone, ethanol, and deionized water. After thorough washing, the surfaces of the substrates were treated with oxygen plasma to remove the adsorbed molecules. After plasma treatment, the glass substrates were covered with a sputtered Cr layer (3 nm) and a sputtered Au layer (50 nm) to form SPR chips.

Biological tissue sections The paraffin-embedded tissue sample of C57BL/6 mouse brain was obtained from Beijing Viewsolid Biotechnology Co., Ltd. Four-micrometer-thick tissue sections with small areas were cut from the paraffin-embedded tissue sample with a microtome (LEICA, RM 2155). The tissue sections were immersed into warm water and spread out and were then transferred onto the as-prepared SPR chips. Afterwards, the SPR chip was soaked in xylene for 3 min to remove most of the paraffin from the surface of tissue sections [18]. Finally, the SPR chip was rinsed with a gradient of alcohol and deionized water, and the SPR chip with the tissue sections was dried in air at

room temperature for subsequent analysis with the HSPRM system. It is worth noting that the removal of paraffin only from the surface layer of tissue sections offers the tissue section both a hydrophilic surface and a paraffin-filled stable matrix. A photograph of the SPR chip locally covered with the mouse brain tissue sections is shown in Fig. 4e.

To investigate the influence of the buffer solution on the tissue-substrate adhesion, a saline solution was prepared by dissolving a given amount of NaCl powder (Sinopharm Chemical Reagent Co. Ltd, China) in deionized water. With the Abbe refractometer, the RI of the saline solution was measured to be 1.36, which will be used for subsequent simulation.

Construction of the HSPRM system

The HSPRM system used in this study was prepared in our laboratory, and its structure, function, and properties are described in detail elsewhere [17]. For ease of understanding, the following is a brief introduction to the HSPRM system. The system consists of a prism-coupled SPR sensor and an upright hyperspectral microscope, which are optically connected via an achromatic imaging lens and a mirror. White light from a high-brightness broadband fiber-coupled lamp is directed to a fiber collimator to produce a collimated beam that passes through a linear polarizer to become polarized. The beam is refracted into the prism coupler at normal incidence and undergoes total internal reflection (TIR) at the metal/glass interface of the SPR chip that is attached to the base of the prism coupler with the RI-matching liquid. The TIR results in evanescent excitation of SPW on the metal surface. The reflected and

scattered light is refracted from the prism coupler and collected by the imaging lens, resulting in a clear SPR image that is adjusted to the horizontal orientation by the mirror for easy observation with the upright hyperspectral microscope. The hyperspectral microscope was assembled in our laboratory using a customized microscope with three different objectives (5×, 10×, 20×) and a push-broom mode hyperspectral imager with 1456 spectral channels and 4.26 megapixels. The resulting HSPRM has a wavelength range of 400–1000 nm, a spectral resolution of up to 0.41 nm, a spatial resolution of up to 2 μm along the SPW vector, and a minimum time of 3.4 s to acquire a hyperspectral SPR datacube. The HSPRM can be used for single-pixel resolved spectral SPR sensing for quantitative analysis and simultaneously for monochrome SPRi sensing for high-resolution visual analytics.

As shown in Fig. 1, the prism coupler used in this work is an equilateral triangular prism made of ZF7LA glass, which is different from the 45° right-angle prism used in our previous study [17]. Under the condition that the light is incident along the normal on the refracting face of the equilateral triangular prism, the SPW with an effective RI equal to $n_p \sin 60^\circ$ can be excited at the glass-substrate/gold-film interface. n_p is the prism RI and exceeds 1.77 in the wavelength range of 400–1000 nm; thus, the effective RI of the SPW is larger than 1.53, which is beyond the tissue RI. This means that higher-order waveguide modes with effective RI values smaller than the tissue RI cannot be excited. With this reason, only one absorption peak can be included in the measured single-pixel reflectance spectrum, corresponding to the SPW at the glass/gold interface, which facilitates the data processing and consequently makes the

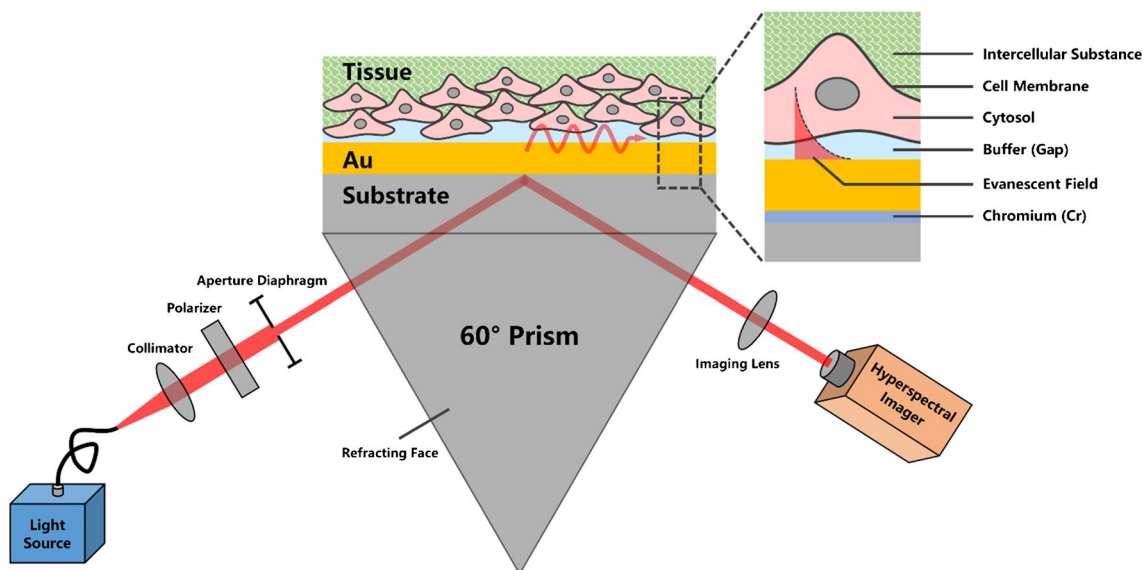


Fig. 1 Schematic diagram of the HSPRM system for stain-free quantitative analysis of biological tissues

tissue analysis easier. If a 45° right-angle prism is used to excite SPW at normal incidence on the refracting face of the prism, the effective RI of SPW is $n_p \sin 45^\circ$, which is less than the tissue RI. In this case, a number of high-order waveguide modes can be excited as long as their effective RI values are between $n_p \sin 45^\circ$ and the tissue RI. As a result, multiple absorption peaks will appear in the single-pixel reflection spectra measured using the HSPRM, and this will complicate the data processing and tissue analysis. The above statements show that the use of equilateral prisms can help to suppress the excitation of higher-order waveguide modes, thereby simplifying data processing and analysis. In addition, a patterned SPR chip with square-shaped and disc-shaped gold films of known sizes was prepared by standard lithography technique for dimensional calibration of SPR images of tissue sections.

Experimental conditions and process

Prior to measurement, the SPR chip with the tissue sections was attached to the base of the prism coupler with the RI-matching liquid. The broadband collimated beam was adjusted to strike the refracting face of the prism and to make TIR occur in the tissue section covered area of the SPR chip. In order to suppress dispersion of light in the prism coupler, the normal incidence on the refracting face of the prism is performed in all measurements of this work. In this case, the TIR angle of the light at the glass-substrate/gold-film interface is 60°. When all the test conditions of the HSPRM system are ready, the *s*-polarized and *p*-polarized hyperspectral images for the dried tissue section were first measured. Afterwards, deionized water was added dropwise on the SPR chip to cover the tissue section; the *s*-polarized and *p*-polarized hyperspectral images were measured again. Note that although the HSPRM system can achieve a spectral resolution of up to 0.41 nm, a spectral resolution of 1.67 nm was chosen during the measurements to make a compromise between shooting speed and imaging quality.

In addition, to determine the excitation conditions for the SPR in biological tissue sections, we first simplified the SPR chip and the tissue section to the multilayer model in Fig. S1(a). After that, we used the five-layer Fresnel reflection model to simulate the reflection spectrum, and the simulation parameters needed are listed in Table S1. It should be noted that during the experiment, the Cr layer of the SPR chip was extremely thin, which had a minimal effect on the SPR. Therefore, this layer was ignored in the simulation. The simulation showed that the SPR cannot be excited with the incident light beam when the tissue-substrate gap is air, while the SPR can be excited when the tissue-substrate gap is water. The simulated spectra under these two conditions are shown in Fig. S1(b) and (c).

Figure 2 illustrates the schematic diagram of detecting biological tissue sections and acquiring the RW/AD image using the HSPRM system. Biological tissue sections are detected with the HSPRM system, and the resulting data cube contains the HSPRM image and the single-pixel spectra. Extracting the spectra of all pixels and using an algorithm to find the RW, the 2D distribution of the RW can be obtained. The RW is related to the RI and AD of tissue sections, and is less affected by scattered light. Using the five-layer Fresnel reflection model and the direct demodulation method to process the RW data, we can quantitatively analyze the tissue-substrate adhesion. Firstly, using the tissue-substrate interface model for simulation, a series of data points can be obtained. Each data point contains a one-to-one correspondence of RW and AD. Afterwards, these data points are fitted to a relationship curve between RW and AD. Finally, the 2D distribution of tissue-substrate AD can be obtained by directly demodulating the 2D distribution of RW with the relationship curve.

Results and discussion

Calibration of the scale bar of the HSPRM image

In prism-coupled SPR microscopy, the image resolution is different in both directions parallel to and perpendicular to the SPW vector, which results from the size compression along the SPW vector direction and consequently results in image distortion. In this work, the image resolution of the HSPRM was calibrated in both directions using the patterned SPR chip prior to tissue section analysis. Figure 3a shows a bright-field optical microscope image of the patterned SPR chip, on which the largest square pattern has a known area of 100 $\mu\text{m} \times 100 \mu\text{m}$ and the smallest disc pattern has a known diameter of 5 μm . Figure 3b displays the corresponding HSPRM image. Obviously, the largest square image in Fig. 3a becomes a rectangle, occupying 125 pixels in the *x*-direction and 63 pixels in the *y*-direction, and thus, each pixel corresponds to a size of 0.8 $\mu\text{m} \times 1.59 \mu\text{m}$. The size is compressed by a factor of 0.5 (namely, $\cos 60^\circ$) in the SPW propagation direction (*y*-direction) [19]. Based on the above result, a calibrated scale bar was obtained for the images measured with the HSPRM, as shown in Fig. 3b. In addition, the smallest disc patterns in Fig. 3a can also be clearly seen in Fig. 3b, where they become ellipsoids closer to each other in the *y*-direction. This means the HSPRM used has a high enough resolution to easily image individual cells in tissue sections.

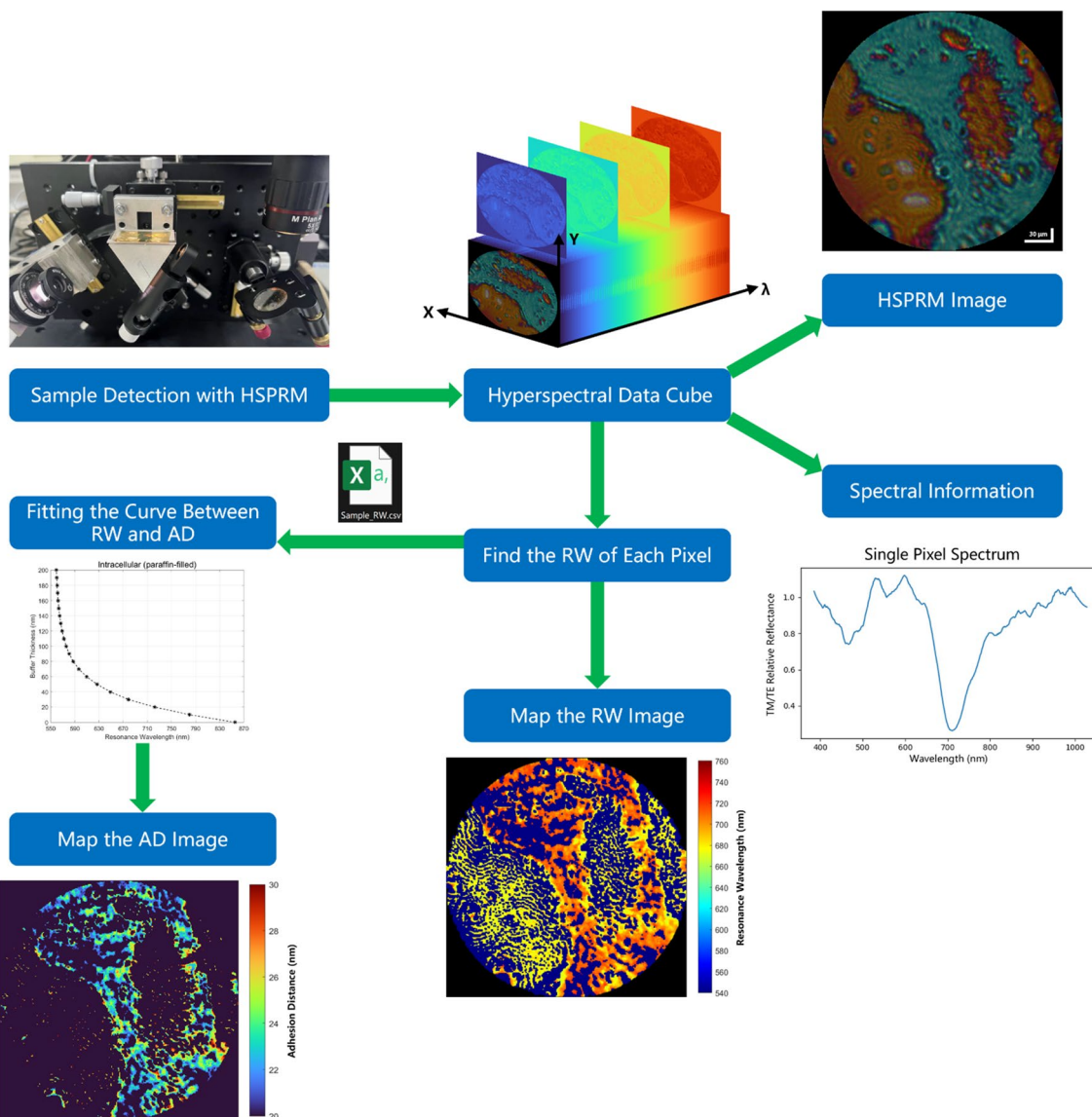
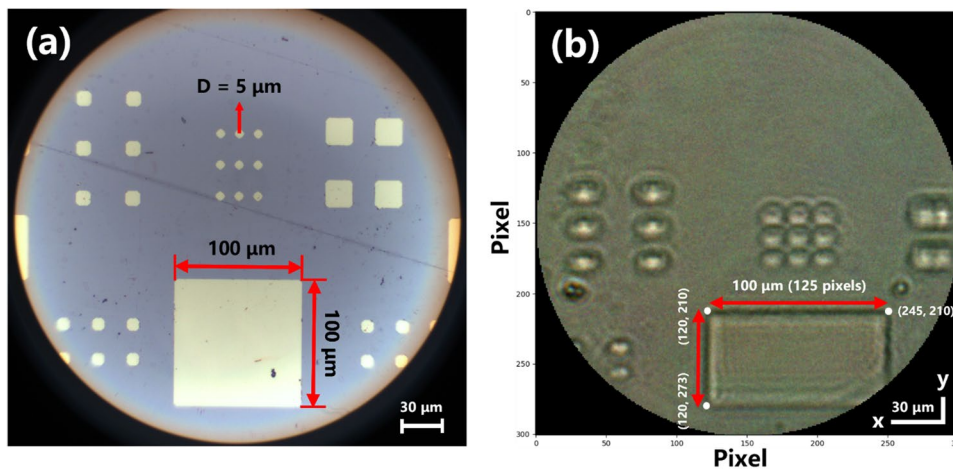


Fig. 2 Illustration of the process of quantitative analysis of biological tissues using the HSPRM system

Fig. 3 a Bright-field optical microscope image of the patterned SPR chip. b HSPRM image of the same chip



HSPRM imaging of mouse brain tissue sections

Figure 4a shows a *p*-polarized image for the dried mouse brain tissue sections measured with the HSPRM, from which some irregular profiles of tissue sections can be seen. Unfortunately, as shown in Fig. 4b, the reflection spectra

of the three pixels labeled in the image do not contain SPR absorption peaks in the wavelength range of 400–800 nm, and thus, the RW values cannot be provided for quantitative analysis. Simulations using experimental parameters based on the five-layer Fresnel reflection model also confirmed that the SPW was not excited with either a bare SPR chip or

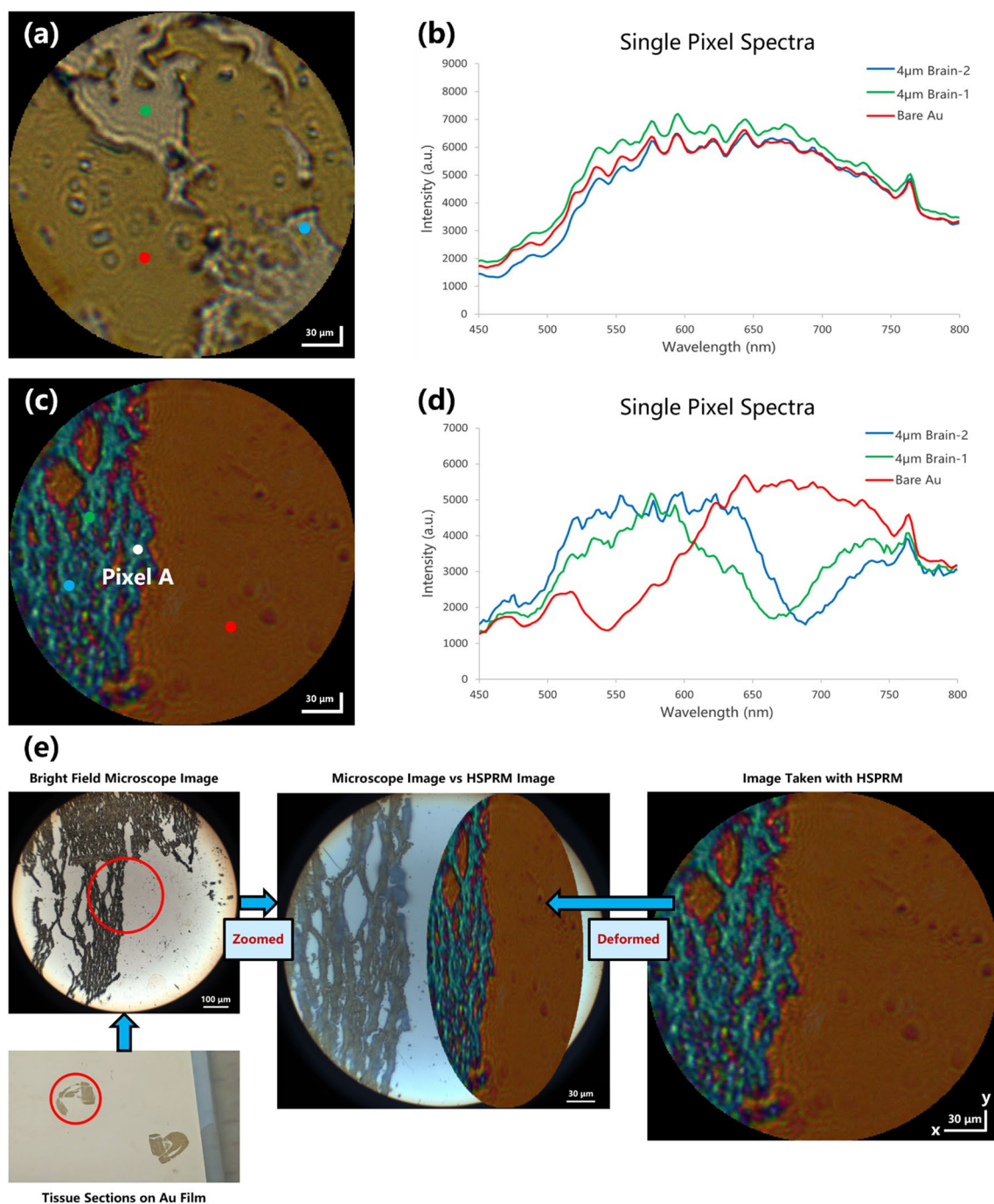


Fig. 4 **a** HSPRM image measured before covering the SPR chip with water. **b** Reflected light intensity spectra of different image pixels in **a**. **c** HSPRM image measured after covering the SPR chip with deion-

ized water. **d** SPR spectra of different image pixels in **c**. **e** Comparison of the bright-field optical microscope image and the HSPRM image of the tissue section

a dried tissue section covered SPR chip. It is clear that the single-pixel reflectance spectra lack useful spectral information. In order to achieve single-pixel RW values, deionized water was added dropwise on the SPR chip to cover the entire area of the chip, and the *s*-polarized and *p*-polarized hyperspectral images were measured again. Note that the *s*-polarized hyperspectral image was used as the reference to suppress the noise of the *p*-polarized image. Figure 4c shows the HSPRM image measured after water coverage, and the reflection spectra of the three pixels marked in the image are shown in Fig. 4d. They are different from those spectra in Fig. 4b and contain well-defined resonance absorption peaks that allow the determination of RW values. In addition, the peak in the area covered by the tissue section had a greater redshift compared to the peak in the area covered with only water. Evidently, this peak redshift results from the tissue section. Figure 4e shows the comparison between the bright-field optical microscope image of the tissue section and its HSPRM image. Figure 4e includes both the wide-field microscope image and high-resolution microscope image of the tissue section. It can be seen from the wide-field image that there are two separated small tissue sections on the SPR chip and the tissue section in a red circle was investigated with the HSPRM. The measured HSPRM image of the tissue section coincides with the selected region of the high-resolution microscope image, and both show that the tissue section has a porous network structure. The bright-field microscope image of the unstained tissue section is grayscale, while its HSPRM image is colorful. The color of the HSPRM images is attributed to the spectral SPR sensing effect, which is able to provide a wealth of information about the tissue-substrate interface.

It is important to note that the thickness of the tissue section under study is about 4 μm , which is much greater than the penetration depth of the plasma field, so the change of the medium at the top of the tissue section from air to water should not affect the reflection spectrum of the tissue-covered area. However, a comparison of the single-pixel spectra between Fig. 4b and d indicates that the change in the medium at the top of the tissue section from air to water results in a distinct SPR absorption peak in the reflection spectrum, which has a large redshift relative to the SPR absorption peak in the chip area not covered by the tissue. The experimental results suggest that the water has diffused into the interface between the tissue and the gold film, forming a thin liquid layer that interacts with the plasmon field.

Acquisition of the 2D distribution of RW and AD

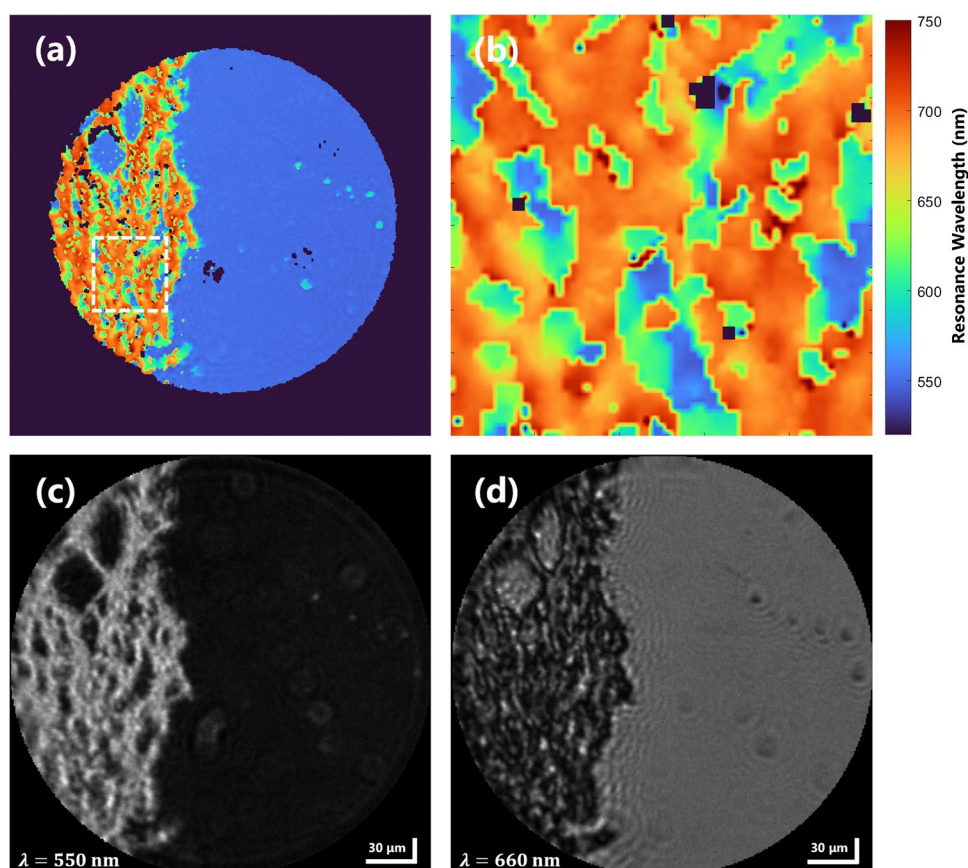
Using the HSPRM image of the tissue section measured in Fig. 4c, the RW values of all pixels of the image can be determined, and then, the 2D distribution of the RW can be plotted. The 2D distribution of RW is more informative

than the conventional grayscale SPR image and can be used for quantitative analysis of the measured sample by simulation based on the five-layer Fresnel reflection model. This is a unique and powerful function of the HSPRM. Figure 5a displays the pseudo-color 2D profile of the RW obtained with the tissue section covered SPR chip, corresponding to the entire HSPRM image in Fig. 4c. As can be seen from Fig. 5a, the RW values of different pixels in the chip region not covered by the tissue are almost the same, approximately equal to 550 nm, while the RW values of different pixels in the tissue-covered region of the chip vary in a wide spectral range from ca. 600 nm to ca. 720 nm. This indicates that the medium at the top of the gold film is unevenly distributed at the microscale. Figure 5b shows a magnified view of the selected area of the RW image in Fig. 5a, and the interfacial microstructure of the tissue-covered area is clearly seen. The HSPRM can provide not only the RW image but also the grayscale image at each of up to 1456 spectral channels. Figure 5c and d show two grayscale images at 550-nm and 660-nm wavelengths, respectively, extracted from the measured hyperspectral datacube. The wavelength of 550 nm is the RW of the gold film without covering the tissue section, which is far from the RW values of the tissue-covered region. In this case, the grayscale image presents the blurred interfacial microstructure. The wavelength of 660 nm is in the RW range of the tissue coverage area of the SPR chip, and the corresponding grayscale image presents a clearer microstructure than that at 550 nm.

Assuming that the tissue-covered region of the SPR chip is a five-layer optical structure composed of a glass substrate, a gold film, a water layer, a phospholipid bilayer (the outermost layer of the tissue), and the tissue section with residual paraffin. The 2D profile of the RW measured in Fig. 5a can be used to derive the thickness distribution of the water layer through simulation based on the five-layer Fresnel reflection model. The water-layer thickness represents the tissue-substrate AD and its 2D distribution reflects the surface micromorphology of the tissue section, which has not been quantitatively studied so far. Previous studies of bioadhesion distance have focused on the cell-substrate system [20], which is simpler than the tissue-substrate system studied in this work. In the five-layer simulation model mentioned above, the phospholipid bilayer has a thickness of ca. 8 nm and RI of ca. 1.50 [21], and the RI of the paraffin-filled tissue section ranges from 1.39 (tissue index) to 1.48 (paraffin index [22]). In order to be able to carry out reasonable simulations, the RI of the paraffin-filled tissue was simplified to be 1.48. This rough approximation could affect the obtained relative thickness of the water film rather than the 2D morphology of the tissue surface.

For easy understanding of the simulation process based on the above five-layer model, Fig. 6a shows the simulated SPR absorption spectra with different thicknesses of the

Fig. 5 **a** Pseudo-color RW image measured after covering the SPR chip with deionized water. **b** Magnified view of the selected area in **a**. **c**, **d** Grayscale images at 550-nm and 660-nm wavelengths, respectively, extracted from the measured HSPRM image



water layer, from which it is seen that increasing the water-layer thickness causes the SPR absorption peak to shift towards shorter wavelengths, due to the weakening of the plasmon field with the tissue section. Figure 6b displays the RW values versus the water-layer thicknesses and the corresponding fitting curve. It is evident that the RW is very sensitive to the water-layer thickness. Therefore, the water-layer thickness can be derived from the measured RW values; this is achieved by adjusting the fitting parameter (i.e., the water-layer thickness) to make the simulated RW equal to the measured value. As an example, Fig. 6c shows the single-pixel SPR absorption spectrum extracted from pixel A of the HSPRM image measured in Fig. 4c and the best-fit spectrum obtained by simulation. The RW values in both the measured spectrum and the best-fit spectrum are 679 nm, and the water-layer thickness is determined to be 30 nm. After obtaining the water-layer thicknesses of all pixels from the HSPRM image in Fig. 4c in the same way, the pseudo-color 2D profile of the tissue-substrate AD was plotted as shown in Fig. 6d. The AD image clearly shows the irregular microstructure that reflects the surface micromorphology of the tissue section. By counting the number of pixels with the same AD value in the image in Fig. 6d, it can be concluded that the tissue-substrate AD ranges from 20 to 35 nm with a peak of 27 nm. Such a nanometric water layer should be

related to the hydrophilic surface of the tissue section, which enables the tissue surface to remain moist, thus creating conditions for the immune binding of the tissue to the substrate if necessary.

In order to further demonstrate the applicability of the HSPRM in quantitative analysis of adhesion between tissue sections and substrates, a saline solution was used to cover the SPR chip instead of deionized water so as to form the saline-filled gap between the tissue section and the substrate, and the tissue-substrate AD was then investigated under the condition that the broadband collimated beam is incident along the normal on the refracting face of the prism. Figure 7a shows the measured HSPRM image, in which the color of the tissue-covered area is different from that of the uncovered area and the contour of the tissue section can be clearly seen. Figure 7b shows three single-pixel reflection spectra extracted from the measured HSPRM datacube, each corresponding to one of the labeled pixels in Fig. 7a. From the spectrum (red curve) for the chip area uncovered by the tissue, the RW was determined to be 650 nm. Given a linear response to bulk RI for each pixel of the HSPRM used, a change of RW from 550 nm for the water-covered gold film to 650 nm for the saline-covered gold film results in a single-pixel RI sensitivity of 3333 nm/RIU. In addition, it can be seen from Fig. 7b that the SPW absorption peak in the tissue-covered region of the chip has a large

Fig. 6 **a** Simulated SPR absorption spectra with different water-layer thicknesses. **b** Resonance wavelengths versus the water-layer thicknesses. **c** Comparison of the simulated reflectance spectrum with the measured SPR absorption spectrum of pixel A in Fig. 4c. **d** 2D distribution of the tissue-substrate AD obtained after covering the SPR chip with deionized water

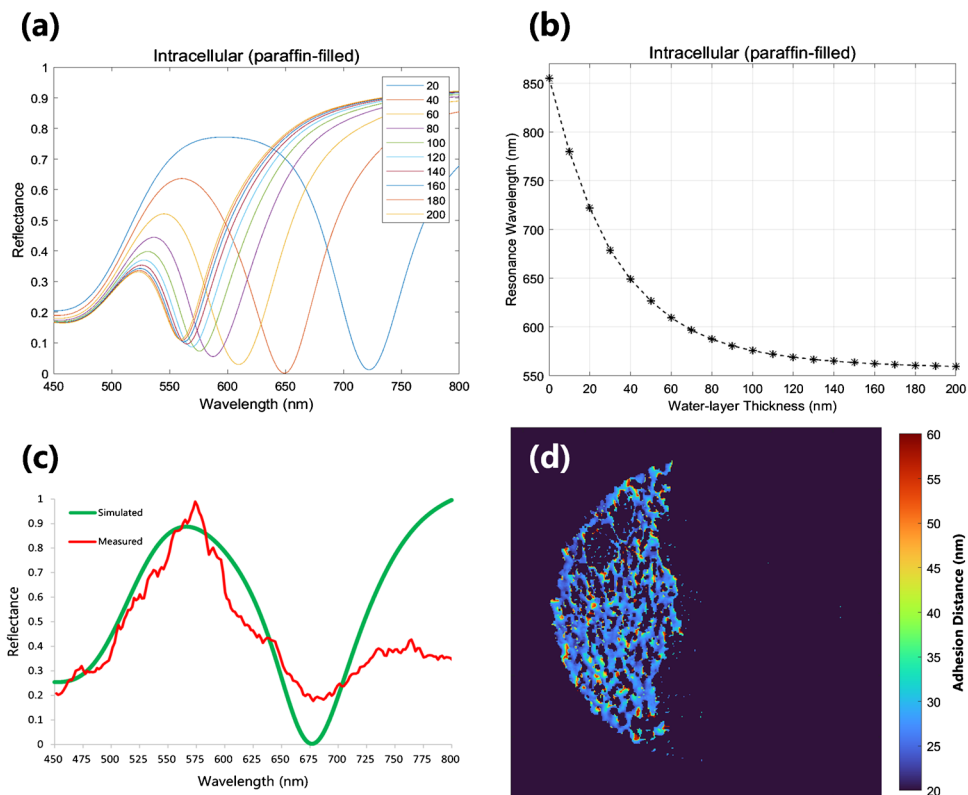
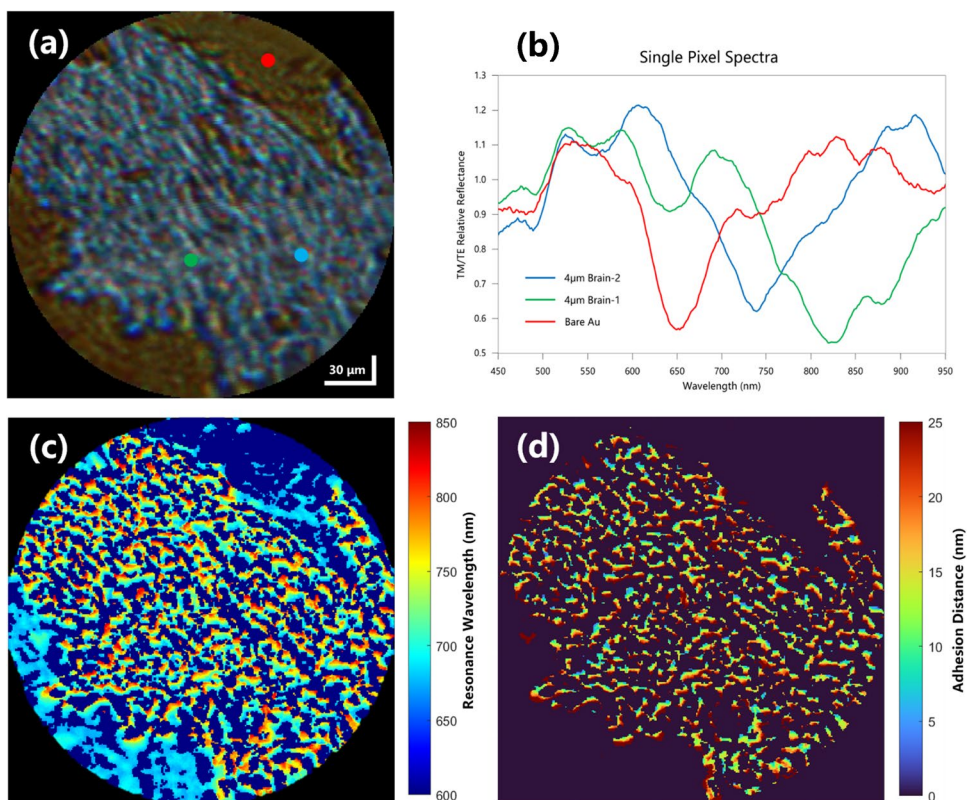


Fig. 7 **a** HSPRM image measured after covering the SPR chip with the saline solution. **b** SPR spectra of different pixels. **c** Pseudo-color RW image obtained from the HSPRM image. **d** 2D distribution of the tissue-substrate AD



redshift relative to the peak in the uncovered region. After the RW values of all pixels in the measured HSPRM image were determined, a pseudo-color 2D profile of the RW was plotted, as shown in Fig. 7c. By fitting the simulated RW to the measured value, the single-pixel-resolved tissue-substrate AD values were obtained. Figure 7d shows the resulting 2D distribution of the tissue-substrate AD. It was concluded by counting the number of pixels with the same AD value in Fig. 7d that the tissue-substrate AD ranges from 4 to 24 nm with a peak of 13 nm. A comparison between Figs. 6d and Fig. 7d indicates that the saline-filled gap between the tissue section and the gold film is smaller than that of the deionized water-filled gap, and it further indicates that the HSPRM used is able to detect changes in the tissue-substrate AD with high spatial resolution.

Conclusion

In this work, the preliminary application of the HSPRM for quantitative analysis of unstained biological tissue sections was demonstrated for the first time. The HSPRM is a newly developed multifunctional optical instrument for surface and interface analysis, which is a perfect combination of hyperspectral imaging, SPR sensing, and traditional microscopy. The HSPRM enables monochromatic and spectral SPR imaging, single-pixel-resolved spectral SPR sensing, and 2D quantification of thin films with the measured RW images. By using the laboratory-made HSPRM system, the surface-deparaffinized mouse brain tissue sections attached to the unmodified SPR chips were investigated under the optimized experimental conditions that include the use of an equilateral triangular prism coupler and the normal incidence on the refracting face of the prism. The HSPRM images of the biosamples were observed in the case of covering the SPR chip with deionized water or saline solution, and the corresponding RW images were obtained. The experimental data combined with the simulation results revealed a nanometric gap between the tissue section and the substrate, which represents the tissue-substrate AD. The 2D distribution of the tissue-substrate AD was then obtained by pixel-by-pixel fitting of the simulated RWs to the measured values. It can be inferred from this work that the nanometric gap between the tissue section and the substrate can seriously interfere with the accurate identification of tumor cells from normal cells in the tissue sample being investigated. From the point of HSPRM-based unstained histopathological diagnosis, the nanometric gap between the tissue section and the substrate is a negative factor that should be inhibited by biomolecular binding at the interface. Due to its high sensitivity, high spatial resolution, high spectral resolution, ultra-high throughput, and strong label-free detection ability, HSPRM

is superior to the existing technique in rapid histopathological diagnosis without staining and has great potential for clinical application.

Supplementary Information The online version contains supplementary material available at <https://doi.org/10.1007/s00216-024-05509-0>.

Acknowledgements We would like to thank Dr. Lichao Zhang for her help in the revision process.

Author contributions Z.M.Q. conceived the concept, designed the HSPRM system, supervised experiments and data analysis, revised the manuscript, and raised funding. B.Y. prepared the tissue-attached SPR chip, conducted experiments, performed modeling and simulation, analyzed the experimental results, and wrote and revised the manuscript. H.Y.T. contributed to the modeling and simulation and the data analysis. Z.W.L. contributed to the construction of the instrument and computational programming. X.X.C. was involved in the results discussion, manuscript revision, and funding acquisition. All authors discussed the results and gave approval to the final version of the manuscript.

Funding This work was supported by the National Natural Science Foundation of China (62121003, 61931018, 62201547) and the National Key R&D Program of China (2021YFB3200100).

Declarations

Ethics approval All animal care and procedures with the C57BL/6 mouse were approved by the Animal Welfare Ethics Committee of Beijing Viewsolid Biotechnology Co., Ltd. And the studies were conducted according to the guidelines for animal experiments by Beijing Association on Laboratory Animal Care.

Competing interests The authors declare no competing interests.

References

- Balaur E, O'Toole S, Spurling AJ, Mann GB, Yeo B, Harvey K, et al. Colorimetric histology using plasmonically active microscope slides. *Nature*. 2021;598:65–71. <https://doi.org/10.1038/s41586-021-03835-2>.
- Eckhard AH, O'Malley JT, Nadol JB, Adams JC. Mechanical compression of coverslipped tissue sections during heat-induced antigen retrieval prevents section detachment and preserves tissue morphology. *J Histochem Cytochem*. 2019;67(6):441–52. <https://doi.org/10.1369/0022155419826940>.
- Gambella A, Porro L, Pigozzi S, Fiocca R, Grillo F, Mastracci L. Section detachment in immunohistochemistry: causes, troubleshooting, and problem-solving. *Histochem Cell Biol*. 2017;148(1):95–101. <https://doi.org/10.1007/s00418-017-1558-4>.
- Rothenhäusler B, Knoll W. Surface-plasmon microscopy. *Nature*. 1988;332:615–7. <https://doi.org/10.1038/332615a0>.
- Yeatman EM, Ash EA. Surface plasmon microscopy. *Electr Lett*. 1987;23(20):1091–2. <https://doi.org/10.1049/el:19870762>.
- D'Agata R, Spoto G. Surface plasmon resonance imaging for nucleic acid detection. *Anal Bioanal Chem*. 2012;405(2–3):573–84. <https://doi.org/10.1007/s00216-012-6563-9>.
- Su Y-W, Wang W. Surface plasmon resonance sensing: from purified biomolecules to intact cells. *Anal Bioanal Chem*. 2018;410(17):3943–51. <https://doi.org/10.1007/s00216-018-1008-8>.

8. Foudeh AM, Trigui H, Mendis N, Faucher SP, Veres T, Tabrizian M. Rapid and specific SPRi detection of *L. pneumophila* in complex environmental water samples. *Anal Bioanal Chem.* 2015;407(18):5541–5. <https://doi.org/10.1007/s00216-015-8726-y>.
9. Sun R, Zhou Y, Fang Y, Qin Y, Zheng Y, Jiang L. DNA aptamer-linked sandwich structure enhanced SPRi sensor for rapid, sensitive, and quantitative detection of SARS-CoV-2 spike protein. *Anal Bioanal Chem.* 2024;416(7):1667–77. <https://doi.org/10.1007/s00216-024-05172-5>.
10. Wang Q, Yin X, Yin P, Ge Y, Wang L, Zhao Y, Zhang H, Zhu A, Yan X, Qiu F, Zhang K, Jiang Y. Research progress of resonance optical fiber sensors modified by low-dimensional materials. *Laser Photon Rev.* 2023;17(5):2200859. <https://doi.org/10.1002/lpor.202200859>.
11. Huo Z, Li Y, Chen B, Zhang W, Yang X, Yang X. Recent advances in surface plasmon resonance imaging and biological applications. *Talanta.* 2023;255:124213. <https://doi.org/10.1016/j.talanta.2022.124213>.
12. Yanase Y, Hiragun T, Kaneko S, Gould HJ, Greaves MW, Hide M. Detection of refractive index changes in individual living cells by means of surface plasmon resonance imaging. *Biosens Bioelectr.* 2010;26:674–81. <https://doi.org/10.1016/j.bios.2010.06.065>.
13. Ma G, Liang R, Wan Z, Wang S. Critical angle reflection imaging for quantification of molecular interactions on glass surface. *Nat Commun.* 2021;12:3365. <https://doi.org/10.1038/s41467-021-23730-8>.
14. Cairós C, Oliva-García R, Siverio G, Trujillo-Sevilla JM, Rodríguez-Ramos JM, Acebes Á. Refractive index estimation in biological tissues by quantitative phase imaging. *Optic Mater.* 2023;142: 114087. <https://doi.org/10.1016/j.optmat.2023.114087>.
15. Zeng Y, Zhou J, Wang X, Cai Z, Shao Y. Wavelength-scanning surface plasmon resonance microscopy: A novel tool for real time sensing of cell-substrate interactions. *Biosens Bioelectr.* 2019;145:111717. <https://doi.org/10.1016/j.bios.2019.111717>.
16. Qi Z-M, Xia S, Wei M, Matsuda H, Zhou H. Systematic characterization of spectral surface plasmon resonance sensor with absorbance measurement. *Appl Optics.* 2007;46(32):7963–9. <https://doi.org/10.1364/AO.46.007963>.
17. Liu Z, Wu J, Cai C, Yang B, Qi Z-M. Flexible hyperspectral surface plasmon resonance microscopy. *Nat Commun.* 2022;13:6475. <https://doi.org/10.1038/s41467-022-34196-7>.
18. Faoláin EO, Hunter MB, Byrne JM, Kelehan P, Lambkin HA, Byrne HJ, Lyng FM. Raman spectroscopic evaluation of efficacy of current paraffin wax section dewaxing agents. *J Histochem Cytochem.* 2005;53(1):121–9. <https://doi.org/10.1177/002215540505300114>.
19. Ahangar SB, Konduru V, Allen JS, Miljkovic N, Lee SH, Choi CK. Development of automated angle-scanning, high-speed surface plasmon resonance imaging and SPRi visualization for the study of dropwise condensation. *Exp Fluids.* 2020;61:12. <https://doi.org/10.1007/s00348-019-2844-9>.
20. Dai S, Yu T, Zhang J, Lu H, Dou J, Zhang M, et al. Real-time and wide-field mapping of cell-substrate adhesion gap and its evolution via surface plasmon resonance holographic microscopy. *Biosens Bioelectr.* 2021;174:112826. <https://doi.org/10.1016/j.bios.2020.112826>.
21. Son T, Seo J, Choi I-H, Kim D. Label-free quantification of cell-to-substrate separation by surface plasmon resonance microscopy. *Optics Commun.* 2018;422:64–8. <https://doi.org/10.1016/j.optcom.2017.10.001>.
22. Cooper PR. Refractive-index measurements of paraffin, a silicone elastomer, and an epoxy resin over the 500–1500-nm spectral range. *Appl Opt.* 1982;21(19):3413–5. <https://doi.org/10.1364/AO.21.003413>.

Publisher's Note Springer Nature remains neutral with regard to jurisdictional claims in published maps and institutional affiliations.

Springer Nature or its licensor (e.g. a society or other partner) holds exclusive rights to this article under a publishing agreement with the author(s) or other rightsholder(s); author self-archiving of the accepted manuscript version of this article is solely governed by the terms of such publishing agreement and applicable law.